Passive Blade Optimization and Evaluation in Off-Design Conditions

Manfred Imiela and Gunther Wilke
German Aerospace Center
Institute of Aerodynamics and Flow Technology
Lilienthalplatz 7, 38108 Braunschweig, Germany
manfred.imiela@dlr.de; gunther.wilke@dlr.de

Abstract

In the present study the effect of twist and anhedral on hover and forward flight performance is analyzed. In forward flight different modelling techniques are assessed with respect to experimental data of the EC1/EC2 rotor before starting the optimization. Subsequently the influence of the trim law on the optimization result is analyzed. Shortcomings of the loose coupling approach which has been used for the optimization are identified when operating conditions approach the boundary of the flight envelope. Finally an optimization using a multi-fidelity approach with multiple design parameters on twist, chord, sweep and anhedral is being presented.

1. Introduction

The improvement of helicopter performance has been a permanent goal for design engineers over decades. Due to the wide range of operations of a helicopter rotor conflicting requirements have to be met at the same time thus making the rotor design a challenging task. Currently the topic is being given increased attention through various national and European projects such as the German research project ECO-HC and the European Clean Sky Green Rotorcraft (GRC) which aims at reducing the environmental impact of an increasing rotorcraft traffic. Several research works have adressed the topic in the last years such as [4] , [8] , [11] , [3].

A framework for the optimization of the rotor blade shape has been presented in [5] where the proposed method has been applied to a model rotor in hover and fast forward flight under moderate loading conditions. Following the industrial specifications given in the aforementioned programs an optimization of a five-bladed full-size rotor in hover and forward flight has been carried out. In previous works of the author such as [6] and [7], twist has been identified as one of the main design parameters. With respect to planform modifications anhedral has been chosen as an additional design parameter.

Following the procedure in [7] hover computations are performed using symmetry boundary conditions while in forward flight only a single blade of the rotor is modelled. Optimizations are carried out on coarse meshes (hover: 100.000 nodes, forward flight: 250.000 nodes), while for verification purposes selected designs are evaluated on fine meshes. In forward flight all blades of the rotor are computed using the chimera technique (hover: 1.4Mio. nodes, forward flight: 10Mio. nodes). For the last optimization case a multi-fidelity approach as described in [12] is used to reduce turnaround times. The performance of the baseline and the optimized configuration are assessed for various flight speeds.

In section 3 three optmizations are carried out in hover. At first the effect of a double-linear twist is investigated (H1). The second optimization case deals with the effect of an anhedral using two design parameters (H2). Subsequently both twist and anhedral are optimized simultaneously in hover (H3). Section 4 deals with the optimization of double-linear twist in forward flight at various flight speeds and blade loadings (F5-F9). Before the optimizations of the full-size rotor (5.5m radius) are conducted different modelling techniques are assessed with respect to the experimental data base of the four-bladed EC1/EC2 rotor (2.1m radius). The optimizations are followed by a comparison of different trim laws and a chapter on convergence issues with respect to the loose coupling. In section 5 nine design variables for twist, chord, sweep and anhedral are investigated in forward flight using the Multi-Fidelity approach as proposed in [12].

2. Optimization Framework

The optimization framework as shown in Figure 1 consists of three elements, i.e. the optimizer, the preprocessing module and the fluid-structure module. The DAKOTA-Software from Sandia Labs [1] is used as optimization tool. It contains different optimization algorithms and steers the overall process by generating the design parameter sets, starting the individual evaluations and collecting the result from each analysis. The parameter set is then passed to the preprocessing unit where the mesh is created. The preprocessor starts with a series of 2D profiles which are lined up on

the quarter chord line along the blade radius. The resulting 3D blade surface is then transferred to the grid generator where the volume mesh of the computational domain is generated. In a last step the monoblock grid is partitioned into multiple blocks in order to make it applicable to a parallel computation.

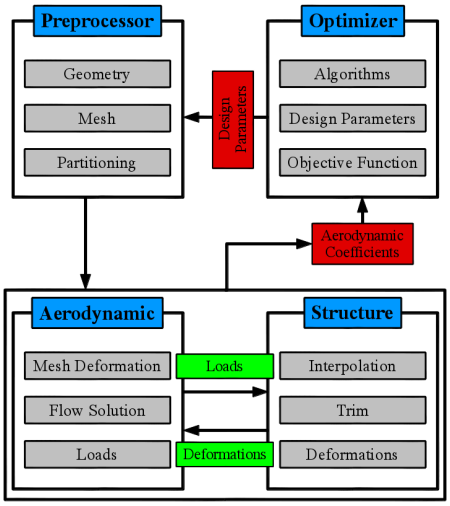

Figure 1: Flowchart of the optimization framework

The fluid-structure module is initiated by a trim computation with HOST. This delivers the dynamic response of the rotor and the elastic deformation which serve as input for the flow computation. After the loose coupling has been carried out for a predefined number of iterations, the aerodynamic coefficients are extracted and passed to the optimizer which decides upon the next set of design parameters. The process is continued until the improvement falls below a predefined threshold.

2.1. Design Variables

The baseline rotor that has been chosen in GRC (workpackage1) is a five-bladed rotor with a radius of 5.5m and consists of two profiles namely the DSA12 from root to 70% blade radius and the DSA9 from 75% up to the blade tip. The inboard part of the blade is rectangular with a blade chord of 0.31m. The outboard part of the blade features a parabolic blade shape. The blade tip chord reduces to 0.103m giving a thrust weighted mean chord of 0.303m. The geometric twist of the baseline blade amounts to $-12°/\mathrm{R}$. No out of plane offset of the quarter chord line (Anhedral) is applied.

Depending on the optimization case twist, anhedral or both are varied. As depicted in Figure 2 two design variables are chosen for each geometric quantity. The twist is modified through ϑ_4 and $\Delta\vartheta_6$ where ϑ_4 defines the absolute twist angle at 90% radius and $\Delta\vartheta_6$ specifies the difference of the twist angles between 90 and 100% radius. Since the absolute twist angle at the

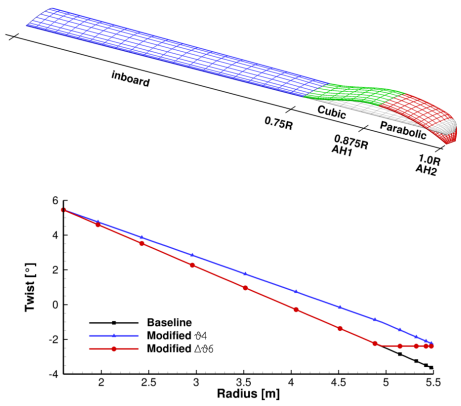

Figure 2: Design Parameters of the optimization process

cut-out (1.6m radius) is fixed (5.455°) this results in a double-linear twist; the first region ranging from 29 to 90 and the second region ranging from 90 to 100% radius. Modifications of the out of plane offset (anhedral) are applied at 87.5% (AH1) and 100% (AH2) radius. While those radial stations correspond to the positions where the maximum offset is reached the changes become effective 12.5% earlier with respect to the radial location, i.e. if AH1 is nonzero the blade starts to bend up- or downwards at 75% blade radius. Between 75% and 87.5% blade radius the out of plane offset is modelled via a cubic function in order to ensure a tangentially constant geometry at those stations. AH2 follows a parabolic function. Positive values denote an upward bending.

3. Hover Analysis

In the current work the Figure of Merit (FM) has been chosen as the goal function for the optimization. In contrary to previous investigations [5] a constraint on the thrust coefficient is implicitly defined. This means that all designs are trimmed to match the thrust design point of $C_T/\sigma = 0.093$. At the end of the chapter all hover optimized designs are evaluated at up to six flight speeds.

3.1. Twist optimization (H1)

The result of the optimization can be seen in Figure 3. Unsurprisingly the optimized design is characterized by a higher twist than the baseline blade. Since we know that a high twist is beneficial in hover this almost trivial result does not bring any new findings. A more interesting result is that the FM already decreases when ϑ_4 reaches values above $-8°$ which is equivalent to approximately $-22°/\mathrm{R}$ and much less than the optimal linear twist of about $-30°/\mathrm{R}$ which is a rough number that can be found in the literature [9] and previous works of the author such as [5].

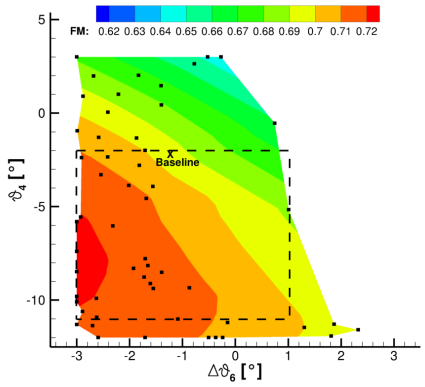

Figure 3: Figure of Merit on coarse mesh as a function of the Twist design parameters ϑ_4 and $\Delta\vartheta_6$ (dashed line shows region of fine grid computation shown in Figure 4)

The reason for this lies in the formulation of the optimization problem. While the thrust in the optimization in [5] was not constrained the designs in the current work are always trimmed to the given design point. A rotor with a linear twist of $-30°$/R would reach a higher FM than the current optimal design. But the high FM would be reached at high C_T/σ values therefore degrading the performance at lower blade loadings. In Figure 3 can be seen that increasing the twist on the outer part of the blade is beneficial. Since the design space has been chosen conservatively the twist on the outer part of the blade is increased up to the bound constraint of $-3°$. Further augmentation of the outboard twist would have resulted in an even higher FM, but would have caused problems in forward flight.

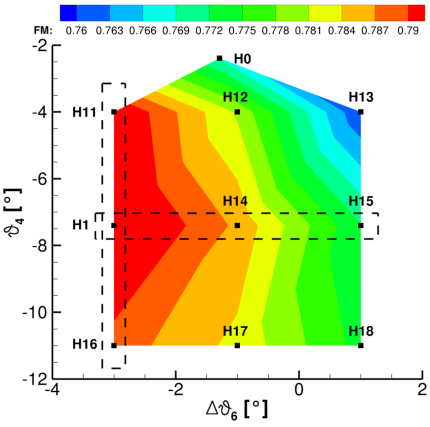

Figure 4: Figure of Merit on fine mesh as a function of the Twist design parameters ϑ_4 and $\Delta\vartheta_6$

Figure 4 presents the objective function on the fine mesh which has been built from the evaluation of ten manually selected samples. H0 represents the baseline and H1 the optimal design point. A qualitative good

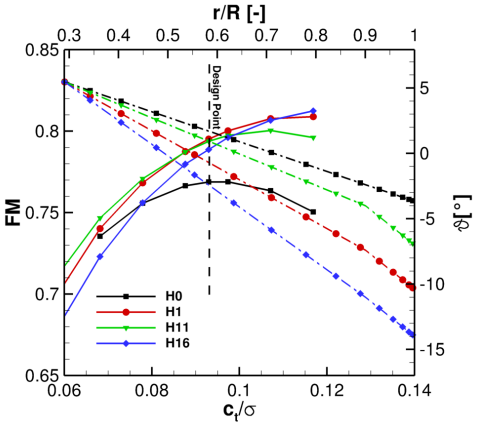

Figure 5: Polars (solid) and twist (dashed) for modified ϑ_4

agreement between the objective function on the coarse and the fine mesh can be observed but the difference of about $\Delta FM = 0.08$ in the computed absolute value for the FM is also evident. The design points H11 to H18 do not depict optimal parameter sets but are chosen so that they are placed almost equidistant around H14. This allows for a detailed analysis of the effect of each design parameter. The variation of ϑ_4 is shown in Figure 5. Clearly the best FM without constraints is reached with the maximum twist (H16). However, the best design with respect to the given design point is H1. It becomes obvious that increasing the twist in the inboard region shifts the maximum FM to higher blade loadings and reduces the FM at lower blade loadings. Figuratively spoken the polars are rotated. This is the reason why a moderate increase in twist is the optimal choice in this case. At the design point ($C_T/\sigma = 0.093$) the FM is increased by 3.5% in comparison to the baseline rotor (H0). At a blade loading of $C_T/\sigma = 0.117$ the FM is increased by approximately 8%. The design parameters and improvement are summarized in Table 1 (see rows Base and H1).

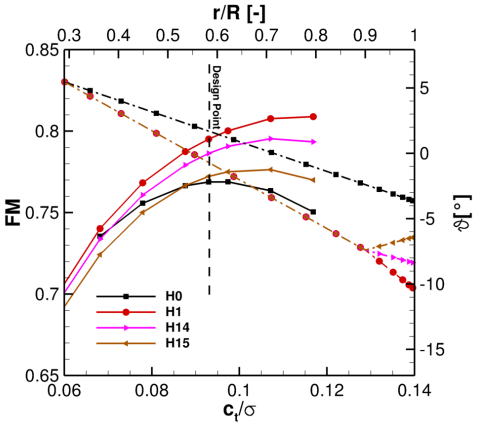

Figure 6: Polars (solid) and twist (dashed) for modified $\Delta\vartheta_6$

Beside the baseline case Figure 6 shows three designs with varation in $\Delta\vartheta_6$. Although the biggest improvements are also found for higher blade loadings, the performance of the designs with increased outboard twist is not degraded at lower blade loadings. Figuratively spoken this time the polars are not rotated as in the first case, but they are rather vertically shifted upwards. Even higher improvements could have been made with $\Delta\vartheta_6$ greater than $-3°$, but at the cost of worsening performance in forward flight as will be seen later.

3.2. Anhedral Optimization (H2)

In the previous section the geometry has been optimized by directly changing the local angle of attack in order to shift the lift generation inboard. In the current section the idea is to modify the out of plane component of the geometry in order to locally increase the miss distance between the current blade and the vortex shed from the previous blade. It would be sufficient in the first place to allow the optimizer to bend the blade up- or downward as it can be seen on blade designs of current helicopters. But in order to give the optimizer more flexibility, two design parameters for anhedral have been used allowing for various combinations of upward- and downward-bending. The results from the previous optimization do **not** serve as a starting point.

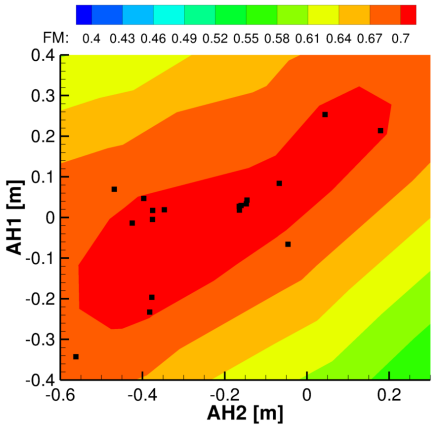

Figure 7: Figure of Merit on coarse mesh as a function of the Anhedral design parameters AH1 and AH2

Figure 7 shows the objective function in the region of the optimal design point. While for AH1 the best designs lie close to zero, for AH2 the optimal designs can be found between -0.1 and -0.2m. If AH1 surpasses values of 0.4 (plus or minus) the value of the objective function drops off quickly. Due to forward flight performance and structural reasons blade designs with small values of anhedral are preferable anyways. The optimal parameter set and performance improvement with respect to the baseline blade are summarized in Table 1 (see rows Base and H2).

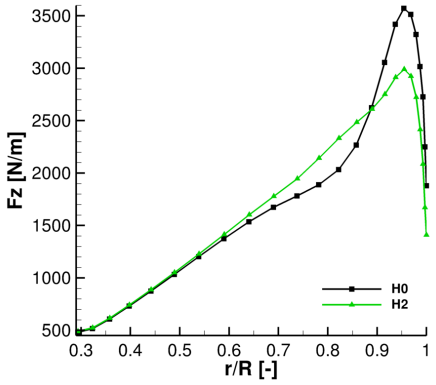

Figure 8: Local blade loading of baseline and H2 optimized blade on coarse mesh

The reason for the improvement can be seen in Figure 8. The baseline blade (H0) shows a noticeable reduction in the radial blade loading gradient between 70 and 85% radius and a steep increase of this gradient from 85 to 95% radius. This is caused by the vortex of the previous blade which changes the local angles of attack - increasing the angle of attack outboard and decreasing it inboard. Since the stream tube through the rotor is contracted, the vortex core is being convected to a location of around 80% radius in this case when it hits the following blade. By bending the blade tip downwards the vortex is released beneath the blade and therfore the miss distance between the blade and the vortex of the following blade is increased. The first anhedral design parameter helps in further increasing this distance by bending the blade upwards. This helps in reducing the effect of the vortex on the local angles of attack and leads to a smooth radial lift distribution. The top and side view of the optimized blade is pictured in Figure 9.

Figure 9: Top and side view of the optimal blade of the anhedral optimization

As can be seen in Figure 10 the optimization of anhedral helped in further increasing the FM at the design point. Compared to the H1 optimization the goal function could be raised by 3.7% which is another 0.3% with respect to the twist optimized blade. Although the twist optimized rotor has the highest FM, the anhedral optimized rotor performs better over a wider range of blade loadings.

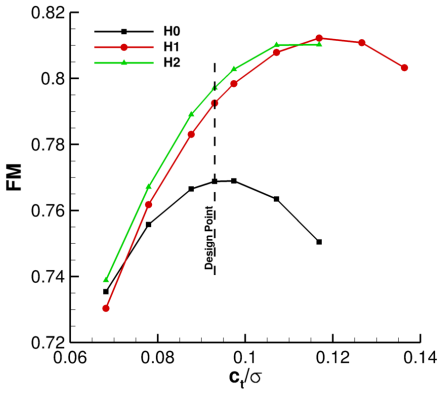

Figure 10: Polar of baseline, twist (H1) and anhedral (H2) optimized blade on fine mesh

3.3. Twist and Anhedral Optimization (H3)

As was demonstrated in the previous sections both optimizations, twist only or anhedral only, have brought a considerable improvement yet caused by different mechanisms. The idea in the current section is to combine the effects of both design parameters and therefore conduct an optimization with both twist and anhedral leading to four design variables in total. Because of the 4D desing space a figure such as Figure 3 or 7 cannot be shown although the optimization is analogous to H1 and H2. The resulting planform can be seen in Figure 11, while the values of the design parameters and the goal function of the baseline and optimized configuration are summarized in Table 1.

Figure 11: Top and side view of the optimal blade of the anhedral optimization

Name	ϑ_4	$\Delta\vartheta_6$	AH1	AH2	ΔFM
Base	-2.4	-1.3	0.0	0.0	0.0
H1	**-7.4**	**-3.0**	0.0	0.0	**+3.4**
H2	-2.4	-1.3	**0.03**	**-0.16**	**+3.7**
H3	**-6.7**	**-3.0**	**0.012**	**-0.062**	**+3.7**

Table 1: Design parameters and and goal function for H1, H2 and H3 optimization

At first glance the combined optimization does not bring any new benfits since the FM is not further improved compared to optimization H2. Looking at the design parameters one can observe that the ϑ_4 is by 1° degree lower than in the twist only optimization case (H1). The anhedral design parameters AH1 and AH2 are reduced to about one third of the values compared to the anhedral only optimization (H2). The superior result of the H3 optimization becomes obvious if the FM is not only considered at the design point but at other blade loadings which is depicted in Figure 12. Although the anhedral is smaller the FM could be raised as much as in the H2 case due to the increased twist. At higher blade loadings the high FM is maintained also due to the increased twist.

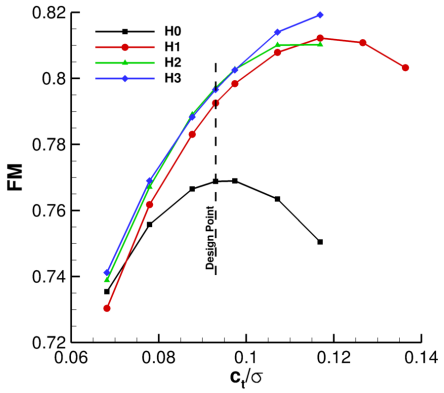

Figure 12: Polar of baseline, twist (H1), anhedral (H2) and twist and anheral (H3) optimized blade on fine mesh

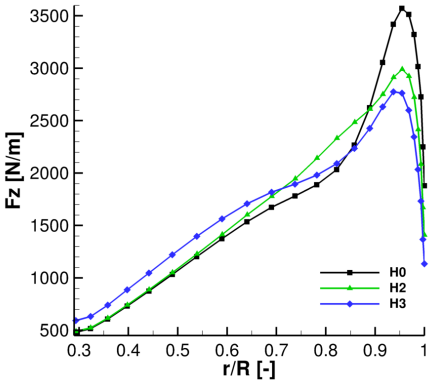

Figure 13: Local blade loading of H2 and H3 optimization on coarse mesh

The local blade loading is plotted in Figure 13. It can be seen that the lift distribution of the current optimization shows a small kink between 75 and 85% radius again. This is probably due to the fact that the optimizer can only change the twist at 90% radius. At first the optimizer reduces the lift at the blade tip and shifts the lift distribution inboard because it is most important. Secondly it tries to produce a smooth lift distribution by manipulating the vortex impingement which is not achieved perfectly. Obviously the optimizer is willing to trade of a greater miss distance for a weaker tip vortex.

3.4. Hover optimized designs in forward flight conditions

The optimizations in hover have been carried out successfully as could be shown in the first part of this paper. Unfortunately the designing engineer is faced with the problem that forward flight and hover are antagonists. Although precaution has been taken in the selection of the design point and by limiting the design space, it cannot be expected that the hover optimized designs yield a performance improvement in forward flight, too. Nevertheless this section deals with the evaluation in forward flight conditions, i.e. the consumed power is assessed for all designs at six different flight speeds with the single blade approach and for further verification at four different flight speeds with the multi-blade approach (for further explanation see [7]). Subsequently the vibration of all designs is analyzed using the following vibration metric (VM):

$$VM = \sqrt{((F_x^{5P})^2 + (F_y^{5P})^2 + (F_z^{5P})^2 + (M_y^{5P})^2 + (M_z^{5P})^2)} \quad (1)$$

The force and moment quantities are obtained from a harmonic breakdown of the aerodynamic forces. More specifically the quantities are the peak-to-peak values of the 5^{th} harmonic for each particular hub force or moment since we are dealing with a five bladed rotor.

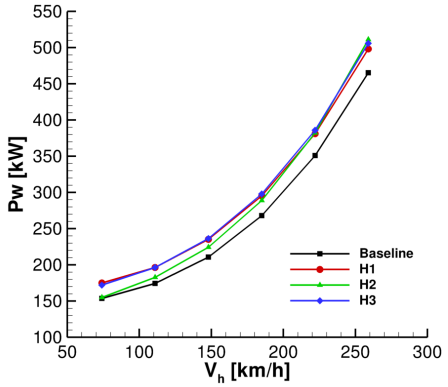

Figure 14: Power vs. flight speed for all configurations on coarse single blade mesh

As expected the baseline rotor consumes the least amount of power as can be seen in Figure 14 and Figure 15. At flight speeds above 200 km/h all optimized configurations consume about an equal amount of power more than the baseline, i.e. approximately between 7 and 10% on the coarse mesh and between 6.5 and 7.5% on the fine mesh. This performance degradation slightly drops for the lowest flight speed of 74 km/h to about 5% on the fine mesh for configurations from H1 and H3 optimization. Surprisingly the H2 configuration is charged with a much lower power penalty

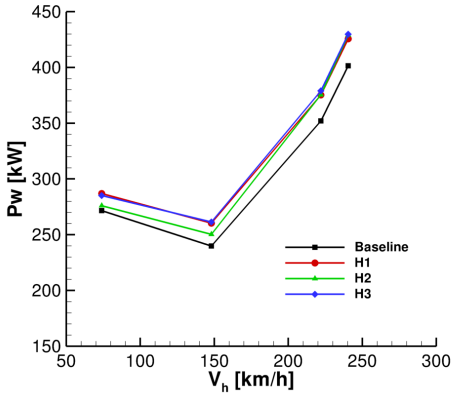

Figure 15: Power vs. flight speed for all configurations on fine mesh

reaching the lowest value of 1.6% on the fine mesh also at the lowest flight speed. Even though the prediction of the consumed power on the coarse mesh deviates severly from the one on the fine mesh, the trends are predicted fairly well. Only for the highest flight speed the order of the different designs with respect to power consumption deviates slightly. Another characteristic that is not well predicted on the coarse mesh is the power increase at lower flight speeds. Even though there is only four evaluations per design on the fine mesh, one can sense the bath tub curve. A characteristic that cannot be seen for the single blade approach on the coarse mesh. This is of course a consequence of the negligence of the influence of the preceding blade. For flight speeds above 150 km/h this effect seems to be small, while for flight speeds below 150 km/h a clear and strong influence can be observed.

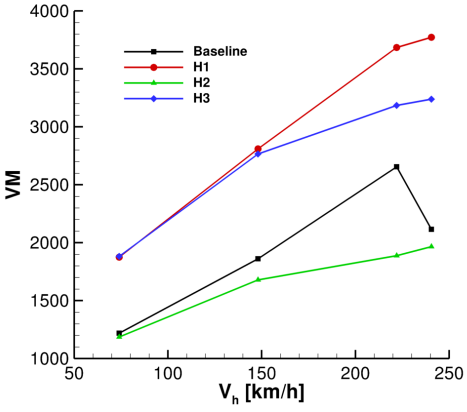

Figure 16: Vibration Metric vs. flight speed for all configurations on fine mesh

Geometry modifications do not only change the performance of a configuration but will also change the vibration level of the rotor. Figure 16 gives an overview of the vibration levels for all hover optimized designs at various flight speeds. As expected vibration lev-

els are higher at high flight speeds and lower at low flight speeds. With respect to the different configurations the highest vibration levels are reached by the twist optimized rotor. It has already been observed in the past that high twist leads to increased vibration. Because of this older blades usually show less twist. Interestingly design H3 shows quite lower vibration levels expecially for higher flight speeds. It seems to be that this is not attributed to the reduced twist compared to H1 design but more likely to the applied anhedral. Even more surprising the only anhedral optimized design (H2) has even lower vibration levels than the baseline rotor. This is very surprising and would need a more detailed analysis that cannot be done in the present work.

4. Analysis in forward flight

The main prerequisite for an assessment of helicopter performance in forward flight is that all configurations are trimmed to the same flight condition. In hover this was achieved if all rotor configuration produced the same lift force. In forward flight the rotor also has to produce a propulsive force. If various flight speeds are considered, the helicopter attitude angle also changes. This means that the orientation of the rotor thrust vector varies for different flight speeds. Table 2 summarizes the trim conditions used for the optimization (No. 6) in GRC and the analyses in off-design conditions. The rotor operates at 347.21 rpm at an altitude of 1800m with a prescribed rotor pitching moment of Mx = 0 Nm. The torque coefficient has been defined as the objective function since it is directly proportional to the required power.

No.	V_h **[km/h]**	F_z **[N]**	F_x **[N]**	α_S [°]
1	74	25657	280	-0.606
2	111	25657	620	-1.364
3	148	25657	1090	-2.425
4	185	25657	1700	-3.786
5	222	25657	2450	-5.443
6	240.5	25657	2870	-5.882
7	259	25657	3330	-7.390

Table 2: Trim conditions for forward flight optimization and off-design conditions

4.1. Model evaluation

Before starting the optimization in forward flight three different models are evaluated with respect to their prediction capability. The crucial aspect is how well each method is able to predict the design sensitivity, i.e. which technique is best suited to predict the impact of a geometry change on the rotor torque coefficient. In order to select a suitable method, the power requirements of two different rotors (EC1 and EC2) at three different flight speeds and various blade loadings have been assessed and compared to the experimental values. Figure 17 shows the performance evaluation of the EC1 and EC2 rotor with the comprehensive rotorcode HOST, the CSD-CFD coupled method (METAR-FLOWer) using a single blade and CSD-CFD coupled method (HOST-FLOWer) modelling the full five bladed rotor by using the chimera technique. While HOST and the single blade approach are used to compute all three advance ratios ($\mu = 0.304; 0.417; 0.509$), the multi blade approach is applied only for the second advance ratio.

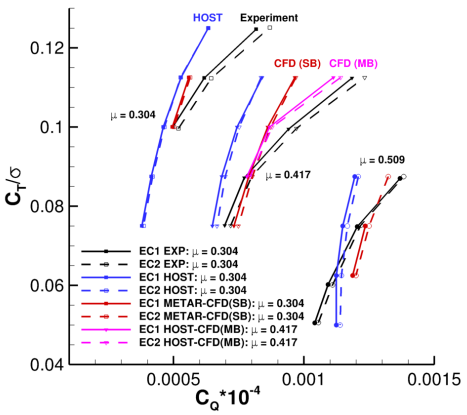

Figure 17: Comparison of comprehensive rotorcode HOST (blue), CSD-CFD single blade (red) and CSD-CFD five-bladed model (pink) for EC1(solid, black)/EC2(dashed, black)

All methods correctly predict the correct order between EC1/EC2 with respect to performance. Results for the lowest advance ratio are least satisfactory. Both methods predict a very small performance difference for all blade loadings which is by far too small compared with the experimental result. For the medium and high advance ratio all methods predict the performance difference between the two rotors satisfactorily for low blade loadings while for high blade loadings the differences vanish for HOST and single blade computations. In terms of absolute power prediction the comprehensive rotorcode computations differ considerably from the experiments. CSD-CFD single blade approach offer a quite reasonable agreement. The best results are obtained with the CSD-CFD multi blade approach. Since the cost of this method is to high to be used inside an optimization loop, the CSD-CFD single blade approach will be chosen for this task.

4.2. Twist optimization (F5 - F9)

In forward flight at first only the influence of double linear twist is analyzed. In order to gain more insight into the sensitivity of the objective function with respect to the design parameters for different flight coniditions a test matrix has been defined including three

different flight speeds and three different blade loadings (see Table 3). For cases F5 - F7 trim law no. 6 has been used, since the flight speed varies only by 10 kts or 18.5 km/h. For cases F8 and F9 the lift force has been changed resulting in a C_T/σ of 0.09 and 0.06 respectively. The results of the optimization are summarized in Table 4 and depicted in Figure 18. The differences in the design parameters at different flight speeds are diminutive but yet consistent. ϑ_4 declines with decreasing flight speed (resulting in a higher inboard twist) while $\Delta\vartheta_6$ grows with decreasing flight speed. That means that twist is increased over the whole blade for decreasing flight speeds - a result which one would expect knowing that in hover a high twist is favorable. The differences for various blade loadings are a little bit greater. For higher blade loadings the twist is increased in comparison to F6, for lower blade loadings the twist is decreased. Although F8 and F9 are equally spaced away from F6 with respect to C_T/σ the differences of the design parameters are greater between F8 and F6 than between F9 and F6. Moreover at the higher blade loading the twist has been changed more severly in the inboard region while at the lower blade loading the change in design parameters can more be found at the outer blade part as can be seen in Table 4. Quite disappointing is the improvement of the objective function which barely exceeds 1.0%.

C_T/σ	**0.09**	**0.075**	**0.06**
V_h **[km/h]**			
259.0		F5	
240.5	F8	F6	F9
222.0		F7	

Table 3: Matrix of optimization cases F5 - F9

	F5	**F6**	**F7**	**F8**	**F9**
ϑ_4	0.99	0.94	0.89	0.58	1.02
$\Delta\vartheta_6$	-1.76	-1.81	-1.88	-1.91	-1.55
ΔPw [%]	1.1	1.0	1.0	0.7	1.2

Table 4: Optimal design parameter set from F5 - F9 and performance improvement with respect to baseline configuration

Figure 19 shows the objective function which results from the computations of the optimization on the coarse mesh. It can be seen that the form of the objective function is parabolic with respect to the design parameters and quickly falls off when the twist is increased too much or in the case with no twist at all. For verification of the optimization nine samples have been computed on the fine mesh (Figure 20) and are compared to the objective on the coarse mesh. Generally the trend on both meshes is equally predicted. Small differences can be observed for low inboard/high

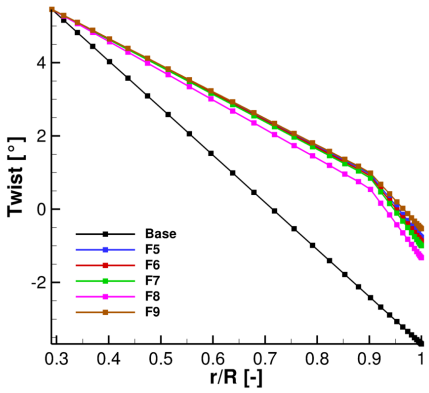

Figure 18: Optimized twist distribution from optimization F5 - F9

outboard twist. In this region the performance prediction for the multiblade approach deviates slightly from the single blade model. The optimal point though is found in the same region.

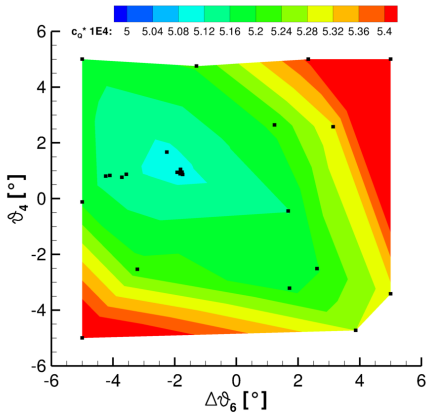

Figure 19: Torque coefficient on coarse mesh as a function of the Twist design parameters ϑ_4 and $\Delta\vartheta_6$

As in the hover case the performance of the optimized configuration is analyzed at various flight speeds. Figure 21 shows the required power of the baseline and optimized configuration (F6) on the coarse mesh as a function of flight speed. As can be seen the optimized configuration performs better at all flight speeds. While the improvement slightly drops at higher flight speeds it steadily increases for lower flight speeds up to difference of 2.2% between baseline and the optimized configuration on the coarse mesh. As in the hover case (Figure 14) it can be seen that the power decreases monotonically with the flight speed due to the single blade simulations which is in contrary to experience from reality. Only three different flight speeds, i.e. 74, 148 and 222 km/h have been evaluated on the fine mesh. Figure 22 shows that the power increases for the lowest flight speed which is more in accordance with experience. The difference between the baseline

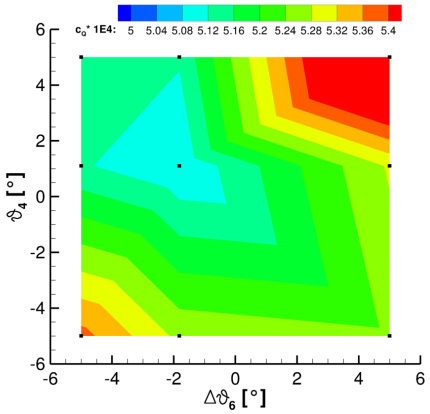

Figure 20: Torque coefficient on fine mesh as a function of the Twist design parameters ϑ_4 and $\Delta\vartheta_6$

and the optimized configuration peaks at 148 km/ to 1.5% and then drops to 0.5% for 74 km/h. Figure 23 indicates the required power as a function of blade loading for the baseline and optimized (F6) configuration on the coarse mesh. For higher blade loadings the improvement declines reaching its lowest value of 0.6 for $C_T/\sigma = 0.09$. For lower blade loadings the performance improvement stays constant.

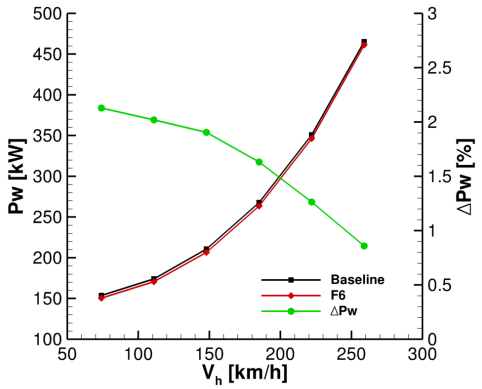

Figure 21: Power vs. flight speed for baseline and optimized (F6) blade on coarse mesh

4.3. Trim law comparison

In GRC a three component trim with prescribed lift and propulsive force and the rotor pitching moment has been used. While this guarantees that all rotors deliver the same lift and propulsive force one cannot be sure that the optimal rotor design does not produce an excessive rolling moment which would change the helicopter attitude leading to a degradation of the complete helicopter configuration. Because of this a different trim law has been used in the German ECO-HC project (termed F10). Here the lift force, the rolling and pitching moment have been fixed ensuring that

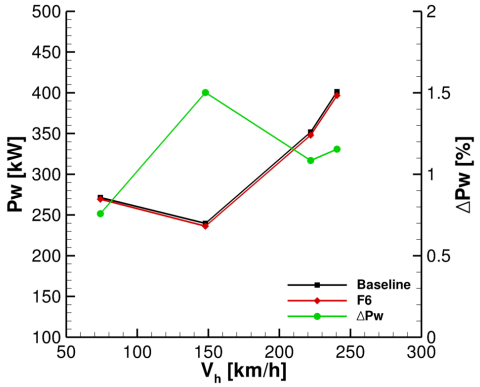

Figure 22: Power vs. flight speed for baseline and optimized (F6) blade on fine mesh

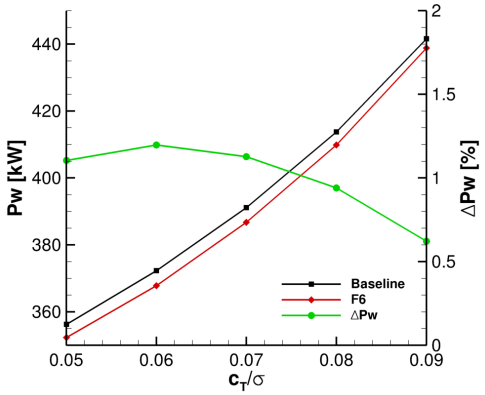

Figure 23: Power vs. blade loading for baseline and optimized (F6) blade on coarse mesh

the attitude of the helicopter fuselage is kept constant for all designs (the shaft angle has also been fixed to $-5.882°$ but is not part of the trim law). The obvious deficit of this trim law is that the propulsive force may vary between different designs. One way to resolve this issue is to use a four component trim where both forces and both moments are prescribed and the shaft angle is allowed to change freely (F11, F13). Of course this is not a natural solution since the shaft angle of a helicopter is usually fixed for one helicopter design. Moreover in reality the shaft angle can only be altered within a small range since there are tight constraints. In order to evaluate the effect of the trim law, optimizations with the values listed in Table 5 have been carried out. The flight speed, alltitude and rpm are chosen as in the F6 optimization case.

No.	F_z **[N]**	F_x **[N]**	M_x **[Nm]**	M_y **[Nm]**
10	25657	-	345	-775
11	25657	2870	0	0
13	25657	2870	345	-775

Table 5: Alternative trim conditions for forward flight optimization

One difficulty in using trim law No.10 is that the designs cannot directly be compared since different blade desings deliver different propulsive forces. One way to overcome this problem is to also use an alternative objective function which is a combination of the required power, the lift and propulsive force. The formulation that has been used in the current section is described in Equation 2

$$Obj = \frac{\frac{Pw}{v_\infty} - F_x}{F_z} \tag{2}$$

where Pw is the power in Watts, v_∞ the flight speed in m/s, F_x the propulsive force in Newton and F_z the lift force in Newton. Basically this represents the ratio between the drag and the lift of the rotor (D/L). The resulting goal function (Obj) is depicted in Figure 24. Both the global characteristic and the optimal design parameters show only small differences. Since the goal function is different from F6 optimization (Figure 19) it is not possible to use the same scale. Another problem is that different sets of design parameters have been computed during the optimization. Those issues partly contribute to the differences between Figure 19 and Figure 24. The values of the design parameters of the baseline and the optimized blade are summarized in Table 6. Compared to the values of the F6 optimization in Table 4 only differences for $\Delta\vartheta_6$ can be observed (0.15°). Surprisingly the improvement of the goal function reaches 2.2%. It should be pointed out that care has to be taken when Equation 2 is used. The reason is that Equation 2 changes the magnitude of the numerator while the denominator is kept constant. This leads to an overprediction of the benefits. If both rotors, baseline and F10 optimized design, are trimmed according to trim law No.6 the improvement is reduced to 1.0%.

Name	ϑ_4	$\Delta\vartheta_6$	**ΔObj**
Base	-2.4	-1.3	0.0
F10	0.9	-1.66	-2.2

Table 6: Design parameters and and goal function for F10 optimization

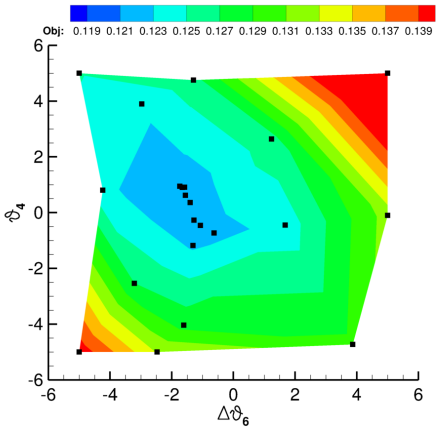

Figure 24: Torque coefficient for optimization F10 on coarse mesh as a function of the design parameters ϑ_4 and $\Delta\vartheta_6$

The result from the optimization with trim No.11 and No.13 are shown in Figure 25 and Table 7. Clearly the result differs only very slightly from the optimization with trim No.6 with respect to the design variables. The only real difference can be observed for the shaft angle α_S which deviates by approximately 1°. The improvement of 1.2% is also very much in accordance with the result from F6. Overall it can be stated that the four component trim yields the same result than the three component reference trim (F6). In terms of convergence of the optimization the four component trim takes slightly longer due to the additional parameter α_S of the trim law. The influence of a prescribed pitching and rolling moment has a negligible influence in this case.

Name	ϑ_4	$\Delta\vartheta_6$	α_S [°]	**ΔPw**
Base	-2.4	-1.3	-6.81	0.0
F11	1.0	-1.86	-6.53	-1.2
F13	1.0	-1.81	-6.12	-1.1

Table 7: Design parameters and goal function for F11 and F13 optimization

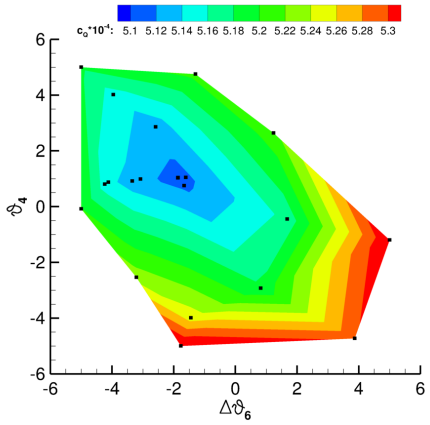

Figure 25: Torque coefficient for optimization F11 on coarse mesh as a function of the design parameters ϑ_4 and $\Delta\vartheta_6$

4.4. Convergence issues

In the previous sections different blade designs have been compared with each other with respect to their performance. This can only be done if the rotors are trimmed **and** the trim is converged. In the present work the loose coupling (or also named delta airloads approach) is used which means that the loads on the one hand and the deformations and control angles on the other hand are exchanged once per revolution. A necessary requirement for a converged coupled and trimmed solution is that each process itself converges, i.e. the trimming has to converge as well as the flow solution (from CFD). The sufficient requirement for a converged coupled and trimmed solution is that the overall process converges, i.e. both individual processes (CFD on the one side and the comprehensive rotorcode trim on the other hand) converge to the same solution. This is usually the case if the control angles vary less than 0.04° between two consecutive trim cycles which is a practical observation (see e.g. [10]).

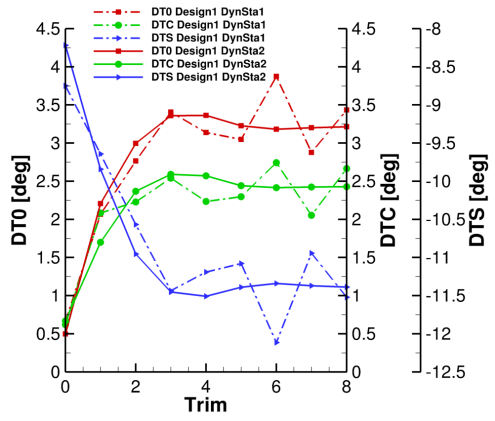

Figure 26: Trim convergence history with and without stall correction (DT0 = collective, DTS/DTC = cyclic)

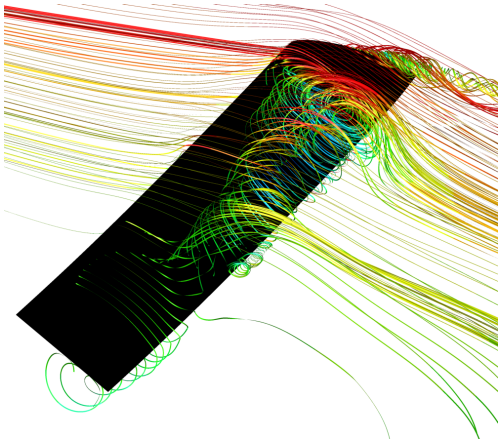

Figure 27: Dynamic stall on retreating blade ($\psi = 274°$

Before the optmizations were carried out with trim law No.6, trim law No.10 was used at a flight speed of 260 km/h. The baseline case worked well, but certain designs posed severe trimming problems as can be seen in Figure 26. By that time a non optimal setting for the dynamic stall correction parameters (DynSta1) was used for the blade element method and so dynamic stall could not be predicted for this model. On the contrary massive flow separation ocured in the CFD flow solution as shown in Figure 27. This led to the problem that the pitching moment of the rotor differed substantially between comprehensive rotorcode and the CFD solution which is depicted in Figure 28. While the peak pitching moment on the comprehensive side just attained -100 Nm/m on the retreating blade side, the peak pitching moment on the CFD side easily reached three times this magnitude. Moreover the strong negative pitching moment changed its location from one trim cycle to the other.

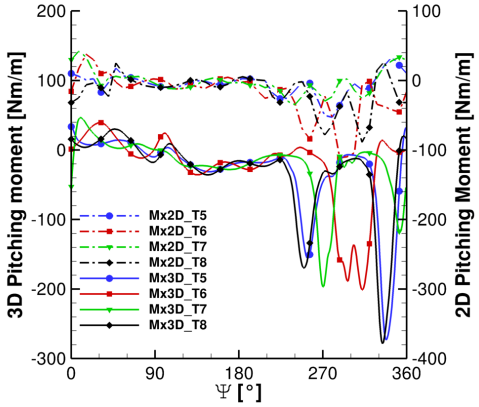

Figure 28: Pitching moment from CFD (solid) and comprehensive rotorcode (dashed) for trim cycles 5 - 8 with DynSta1

A lot of remedies were tried to improve the convergence; amongst them to reduce the time step on the CFD side or to use different relaxation techniques,

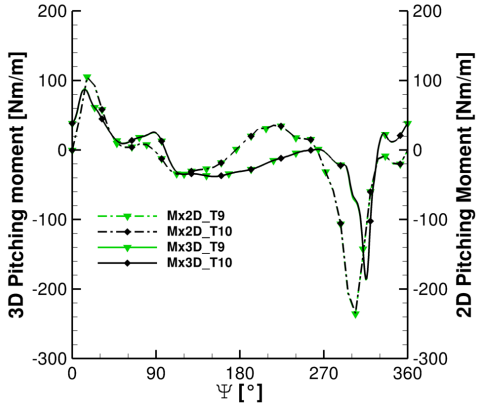

Figure 29: Pitching moment from CFD (solid) and comprehensive rotorcode (dashed) for trim cycles 9 - 10 with DynSta2

but none of them led to an overall converged solution. The measure which finally brought success was to use a modified set of dynamic stall correction parameters (DynSta2) for the comprehensive rotorcode. This improved the prediction of the pitching moment on the comprehensive side and therefore both codes converged step by step to the same solution. Figure 29 shows the CFD and the comprehensive rotocode pitching moment for the last two trim cycles. Apparently this time the magnitude of the negative peak pitching moments are alike. Also the pitching moment does not change between two trim cycles.

5. Multi-Parameter optimization in forward flight (F16)

The optimizations in section 4 have shown that there is only limited potential for improving the rotor performance in forward flight by only optimizing the twist of the blade. Therefore this section deals with a multi-parameter optimization with nine design variables including twist, chord, sweep and anhedral. The blade tip starts at 80% radius. The twist and planform are modelled using NURBS functions with control points at 50, 90 and 100% radius. For chord, sweep and anhedral only the control points at 90 and 100% can be modified, while for twist also the control point at r/R = 0.5 is allowed to move. Negative sweep values signify an aft sweep of the quarter chord line, negative anhedral values denote a downward bending of the quarter chord line. An optimization with nine design variables in forward flight is too costly even with a single blade approach. Therefore this optimization has been done using the multi-fidelity optimization technique as described in [13] which significantly reduces the turnaround time for the optimization. More specifically METAR has been used as low-fidelity and Euler as mid-fidelity method. The optimization results are thus the same as they would have been obtained with a pure Euler approach. Concerning the trim and the goal function the optimizations have been carried out as in the previous section (F6). The resulting blade shape is depicted in Figure 30 and the position of the NURBS control points and the optimal values are listed in Table 8. The result has been checked with high-fidelity methods, i.e Navier-Stokes computations on fine meshes as in F6 and H1 respectively.

Design Parameter	Position [r/R]	F16
Twist1	0.5	3.455
Twist2	0.9	2.455
Twist3	1.0	-0.968
Chord1	0.9	0.310
Chord2	1.0	0.153
Sweep1	0.9	-0.029
Sweep2	1.0	0.310
Anhedral1	0.9	0.051
Anhedral2	1.0	0.031

Table 8: Optimal design parameters of F16 optimization

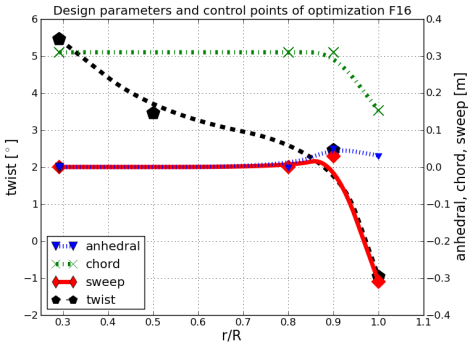

Figure 30: Parameterization and optimal design parameters of F16 optimization

Figure 31: Optimal blade planform from F16 optimization: Top- and sideview

The resulting planform can be seen in Figure 30 and 31. The overall twist changed only slightly in comparison to the twist of the F6 optimization. However the distribution is different. Although in both cases the twist is increased towards the tip this effect is more pronounced in the current optimization (twist angle at 90% radius for F6 = 0.94°; for F16 = 1.76°). The chord is reduced towards the tip since this reduces the blade tip loading and thus the tip vortex. A result which has also been found by other researchers, e.g. [2]. The

strong backward sweep on the outer blade region is counteracted by a mild forward sweep between 80 and 90% radius. The sweep helps to reduce the wave drag on the advancing blade side and improves the radial blade loading through the elastic torsion. The dihedral on the outer blade part looks unconventionally at first glance but is inline with other investigations such as [4]. Experience from other optimizations show that a strong dihedral leads to a severe degradation of the performance in forward flight, but mild dihedral improves the performance. In order to clarify the effects of each design parameter a more detailed analysis would be needed. Instead here the performance in hover and low forward flight speed conditions will be evaluated.

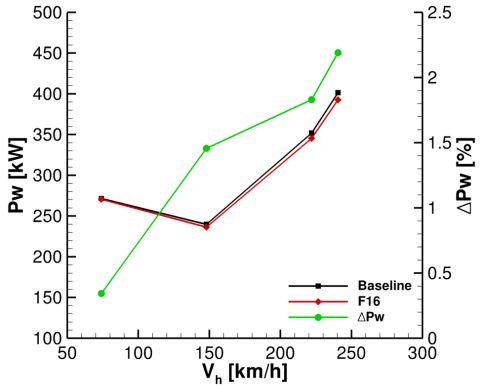

Figure 32: Power vs. flight speed for baseline and optimized (F16) blade with Navier-Stokes computation on fine mesh

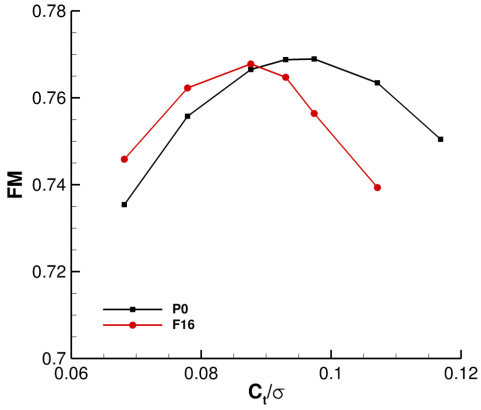

Figure 33: FM polar of baseline and F16 optimized rotor

The performance of the optimized configuration at the design point (trim No.6) is improved by 2.2% with respect to the baseline as can be seen in Figure 32. For lower flight speeds the improvement decreases stedily to 0.3% at 74km/h. The hover performance is depicted

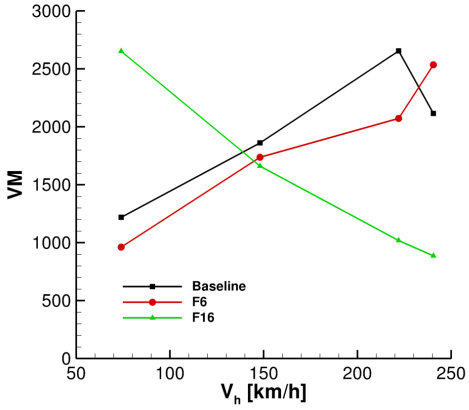

Figure 34: Vibration Metric vs. flight speed for baseline, F6 and F16 configuration on fine mesh

in Figure 33. As expected the FM is decreased at the design blade loading of $C_T/\sigma = 0.093$. Also for higher blade loadings the hover performance is severely degraded. However at lower blade loadings the performance is considerably increased. Figure 34 shows the vibration metric (VM) for the baseline, F6 and F16 optimized configuration. As one would expect VM is lower for the F6 configuration since the twist has been reduced. VM of the F16 configuration is in contrary to experience since the highest VM values are found at low flight speed and vice versa.

6. Conclusion

This paper summarizes the work of two projects namely the German research project ECO-HC and the European Clean Sky Green Rotorcraft project (GRC). It shows that blade planform and twist optimization with the aim of increasing helicopter performance resulting in reduced power requirements is a challenging task. While acceptable improvements can be achieved for each individual flight condition, i.e hover and forward flight, the potential improvement of a combined optimization for both flight conditions is very limited. This means that an important point in the design phase is the definition of a detailed mission profile for the helicopter upon which the engineer can decide over the proportion between both flight conditions. With respect to each flight condition it could be shown that anhedral has a very beneficial effect in hover. Indeed anhedral leads to a performance degradation in forward flight, but the performance decrease is stronger if the twist is increased in order to reach the same benefit in hover. Optimization of twist and anhedral combines both beneficial effects in hover and slightly decreases vibration levels at higher flight speeds. The foward flight performance, however, is degraded as much as in the only twist case. Although being a trivial finding it should be emphasized that the choice of the parameterization is absolutely crucial and probably one of the most im-

portant aspects of planform optimization. In forward flight the performance can be enhanced by reducing the twist. Not only is this in contrary to the hover demand but also the improvements are diminutive when only twist is considered. If multiple parameters are optimized at the same time the improvement can be raised but are still not tremendous. The choice of the trim law does not play such an important role as suspected before having done the analysis. Trim law No.6 is preferred by the author since both lift and propulsive force are trimmed which means that rotors are directly comparable and the additional parameter α_S in the trimming process is avoided. When trim law No.10 has to be used Equation 2 provides an effective way to make rotors comparable, but care has to be taken when it comes to a quantification of the improvements. Since potential performance improvements by optimization of planform parameters are small the author would like to point out that the optimization of the acoustic footprint and the vibratory hub loads are equally important and should therefore also be included in the optimization process. The latter has been considered in a first attempt through the analysis of the vibration metric. Yet this should be investigated in much more detail.

7. Acknoledgements

This research activity has been funded by the EU through the Clean Sky Green Rotorcraft initiative and the German Federal Ministry of Economy and Technology (BMWi) through ECO-HC project. 20H0803

References

[1] B. Adams. The dakota toolkit for parallel optimization and uncertainty analysis. In *SIAM Conference on Optimization*, Boston, MA, May 2008.

[2] K. Collins, J. Bain, N. Rajmohan, L. Sankar, T. A. Egolf, R. D. Janakiram, K. Brentner, and L. Lopes. Toward a high-fidelity helicopter rotor redesign framework. In *American Helicopter Society 64th Annual Forum*, 2008.

[3] A. Dumont, A. LePape, J. Peter, and S. Huberson. Aerodynamic shape optimization of hovering rotors using a discrete adjoint of the rans equations. In *American Helicopter Society 65th Annual Forum*, 2009.

[4] M. Hollands, M. Kessler, and E. Krämer. Influence of an-/dihedral and of different blade-shapes on performance and aeroacoustics of an isolated rotor. In *38th European Rotorcraft Forum*, 2012.

[5] M. Imiela. High-fidelity optimization framework for helicopter rotors. In *35th European Rotorcraft Forum*, 2009.

[6] M. Imiela. Investigation of aeroelastic effects for a helicopter main rotor in hover. In *36th European Rotorcraft Forum*, 2010.

[7] M. Imiela. High-fidelity optimization framework for helicopter rotors. *Aerospace Science and Technology*, 23:2–16, Dec 2012.

[8] C. Johnson and G. N. Barakos. A framework for the optimization of a berp-like blade. In *38th European Rotorcraft Forum*, 2012.

[9] J. G. Leishman. *Principles of Helicopter Aerodynamics*. Cambridge University Press, New york, 2nd edition, 2006.

[10] K. Pahlke and B. G. van der Wall. Chimera simulations of multibladed rotors in high-speed forward flight with weak fluid-structure-coupling. *Aerospace Science and Technology*, 9:379–389, Mar 2005.

[11] A. Visingardi, L. Federico, and M. Barbarino. Blade planform optimization for a dual speed rotor concept. In *38th European Rotorcraft Forum*, 2012.

[12] G. Wilke. Variable fidelity optimization of required power of rotor blades: Investigation of aerodynamic models and their application. In *38th European Rotorcraft Forum*, 2012.

[13] G. Wilke. Multi-objective optimizations in rotor aerodynamics using variable fidelity simulations. In *39th European Rotorcraft Forum*, 2013.